JACS
JOURNAL OF THE AMERICAN CHEMICAL SOCIETY

pubs.acs.org/JACS

Article

Direct SARS-CoV-2 Nucleic Acid Detection by Y-Shaped DNA Dual-Probe Transistor Assay

Derong Kong, Xuejun Wang, Chenjian Gu, Mingquan Guo, Yao Wang, Zhaolin Ai, Shen Zhang, Yiheng Chen, Wentao Liu, Yungen Wu, Changhao Dai, Qianying Guo, Di Qu, Zhaoqin Zhu, Youhua Xie, Yunqi Liu, and Dacheng Wei*

Cite This: J. Am. Chem. Soc. 2021, 143, 17004−17014

Read Online

ACCESS | Metrics & More | Article Recommendations | Supporting Information

ABSTRACT: Rapid screening of infected individuals from a large population is an effective means in epidemiology, especially to contain outbreaks such as COVID-19. The gold standard assays for COVID-19 diagnostics are mainly based on the reverse transcription polymerase chain reaction, which mismatches the requirements for wide-population screening due to time-consuming nucleic acid extraction and amplification procedures. Here, we report a direct nucleic acid assay by using a graphene field-effect transistor (g-FET) with Y-shaped DNA dual probes (Y-dual probes). The assay relies on Y-dual probes modified on g-FET simultaneously targeting ORF1ab and N genes of SARS-CoV-2 nucleic acid, enabling high a recognition ratio and a limit of detection (0.03 copy μL^{-1}) 1−2 orders of magnitude lower than existing nucleic acid assays. The assay realizes the fastest nucleic acid testing (~1 min) and achieves direct 5-in-1 pooled testing for the first time. Owing to its rapid, ultrasensitive, easily operated features as well as capability in pooled testing, it holds great promise as a comprehensive tool for population-wide screening of COVID-19 and other epidemics.

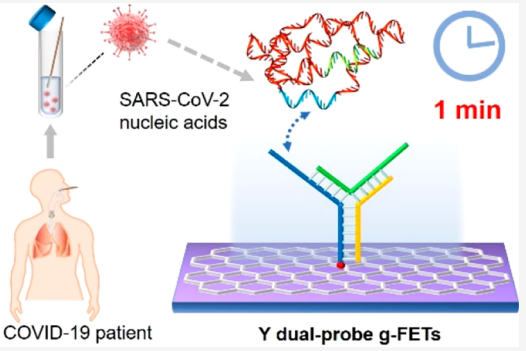

INTRODUCTION

Coronavirus disease 2019 (COVID-19) is an infectious disease caused by severe acute respiratory syndrome coronavirus 2 (SARS-CoV-2).[1−3] The high transmission rate and high proportion of asymptomatic infections have led to the evolution of a global pandemic.[4] With the spread of variants and the slow promotion of the vaccinations in many areas of the world, there is an urgent, massive, and worldwide demand for a comprehensive assay method to rapidly and accurately identify and isolate infected individuals from a large population, so as to curb the transmission of SARS-CoV-2.[5−7]

Currently, there are two types of COVID-19 diagnostic methods, serological and viral nucleic acid tests.[2,4] Serological tests, which directly detect antibodies or antigenic viral proteins, can obtain results rapidly.[8,9] In most cases, they can correctly detect only one-half to three-quarters of infections with false negative results, especially when testing presymptomatic or asymptomatic individuals.[6] Nucleic acid tests include quantitative reverse transcription polymerase chain reaction (qRT-PCR),[10−13] isothermal amplification,[14−21] clustered regularly interspaced short palindromic repeats (CRISPR),[22−25] etc., and are more accurate. Among them, qRT-PCR has been regarded as a gold standard for COVID-19 diagnoses and detects trace amounts of viral nucleic acids. Nevertheless, existing nucleic acid tests normally require extraction and amplification procedures, which need skilled operators, specialized facilities, dedicated laboratories, and a long reaction time, up to 2−4 h.[26,27] Screening tests have different purposes and demands from COVID-19 diagnoses. The screening tests should be accurate while having greater demands on the speed of reporting and the frequency of testing.[28,29] To improve the efficiency of nucleic acid tests in large-scale screening, researchers pool (or combine) samples and test them together.[30,31] However, the nucleic acid pooled testing leads to the "dilution" of the infected specimen(s) and increases the possibility of false negative results. To ensure the accuracy, the pooled testing needs more amplification cycles. Therefore, existing serological and nucleic acid testing methods fail to simultaneously meet the demands of COVID-19 screening in diagnostic accuracy and testing speed, which is not conducive to epidemic prevention and control.

As a promising assay platform, field-effect transistors (FETs) achieve detection of trace biological analytes by monitoring the changes in the conductivity of the semiconductor channel, which are originated from chemical or physical perturbations

Received: June 18, 2021
Published: October 8, 2021

https://doi.org/10.1021/jacs.1c06325
J. Am. Chem. Soc. 2021, 143, 17004−17014

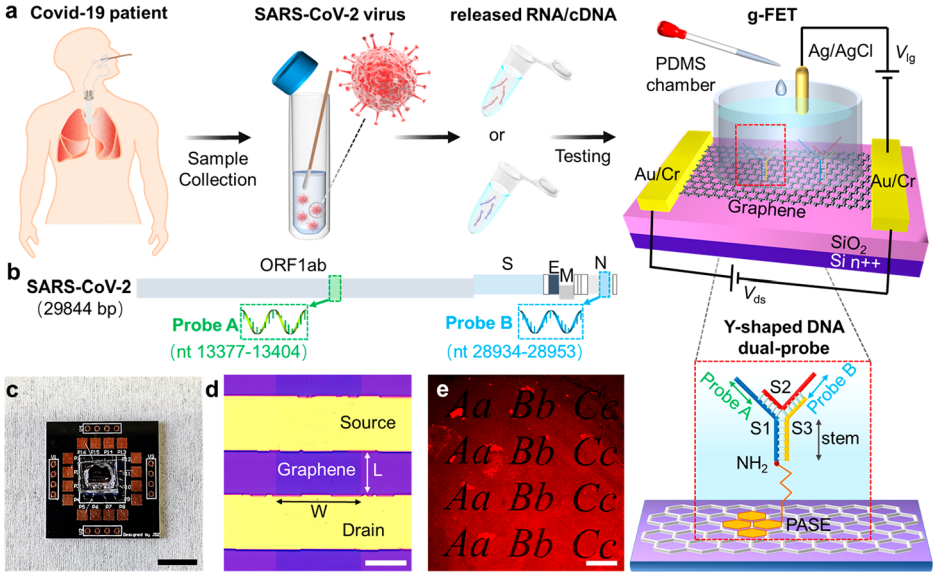

Figure 1. Fabrication and characterization of a Y-dual probe g-FET biosensor. (a) Schematic diagram of a Y-dual probe g-FET biosensor and the workflow of SARS-CoV-2 nucleic acid testing. (b) Selected viral sequences and the targeted positions of the probes in detecting SARS-CoV-2 nucleic acid. ORF1ab: nonstructural polyprotein gene; S: spike glycoprotein gene; E: envelope protein gene; M: membrane protein gene; N: nucleocapsid protein gene. The numbers are the genome location of SARS-CoV-2 NC_045512 in GenBank. (c) Photograph of a packaged device. The scale bar is 1 cm. (d) Optical microscope image of the graphene channel. The scale bar is 30 μm. (e) Fluorescence image of the Cy3-conjugated Y-dual probe on graphene. The scale bar is 250 μm.

relating to specific interactions between recognition elements and analytes.[32−35] After being functionalized with DNA probes as the recognition element, the FET biosensing platforms have great potential in nucleic acid testing for epidemic screening, owing to advantages such as rapid response, efficient signal transduction, label-free detection, easy operation, high integration, and portability.[36−47] However, the routinely used flexible single-stranded DNA (ss DNA) probes are inclined to undergo undesired aggregation and entanglement at the sensing interface of the conducting channel, resulting in the inactivation of the ss-DNA probes and influencing the sensitivity.[48,49] Thus, in the nucleic acid assay, the detectable concentration of DNA probe-based FET biosensors rarely reaches the aM (1 aM = 10^{-18} M) level,[38,47] equivalent to ∼60 copies in 100 μL. In the case of COVID-19 testing, SARS-CoV-2 nucleic acids have a genomic sequence up to ∼30 kilobases.[3] They easily form complicated secondary conformation structures, which limit the accessibility of ss-DNA probes to the target sequence. In view of the above reasons as well as low viral load in real-world samples,[50] the ss-DNA probe-modified FET sensors lack the sensitivity for an unamplified COVID-19 nucleic acid assay. Direct SARS-CoV-2 nucleic acid testing is still absent in clinical applications.

Herein, we report a direct SARS-CoV-2 nucleic acid detection assay by using a graphene field-effect transistor (g-FET) with Y-shaped DNA dual probes (Y-dual probes). Owing to the synergy effect of the two probe sites simultaneously targeting the ORF1ab and N gene regions, g-FET biosensors have a higher recognition ratio toward SARS-CoV-2 nucleic acids with a limit of detection (LoD) down to 3 copies in 100 μL of testing solution. This assay avoids nucleic acid extraction and any polymerase chain reaction or other reaction-based amplification, achieving high sensitivity and rapid testing simultaneously. In the case of nasopharyngeal swab samples, a direct nucleic acid assay is realized even when the samples have low viral load with a cycle threshold (Ct) value up to 40.4. The average diagnostic time reaches ∼40 s, 1−3 orders of magnitude faster than existing technologies of nucleic acid assays. Owing to the ultrahigh sensitivity, Y-dual probe g-FET biosensors correctly identify positive samples in 5-in-1 pooled testing without amplification, appropriately matching the demands of wide-population screening of epidemics such as COVID-19.

RESULTS AND DISCUSSION

Y-Dual Probe g-FET Biosensors. The workflow of a direct SARS-CoV-2 nucleic acids testing assay is illustrated in Figure 1a. The Y-dual probe is one-step assembled from three DNA single strands (S1, S2, S3, Table S1) in Tris-EDTA (TE) buffer and consists of two built-in capture probes extended from S1 and S2. The Y-dual probe includes two different embedded probes (probe A and probe B) that target the ORF1ab gene (nt 13377−13404) and N gene (nt 28934−28953) regions of SARS-CoV-2 nucleic acid, respectively (Figure 1b). Formation of the Y-dual probe is verified by 10% native polyacrylamide gel electrophoresis, showing the expected gel mobility (Figure S1).

The device is configured as a liquid-gated FET with a PDMS chamber on a chemical-vapor-deposited graphene channel (Figure 1c). The dimensions of the channel sensing area are 30 × 60 μm^2 (Figure 1d). The Y-dual probes are anchored on the graphene via the linker molecule 1-pyrenebutanoic acid succinimidyl ester (PASE) through noncovalent $\pi-\pi$ interactions and *N*-hydroxysuccinimide cross-linking reactions (Figure S2).[36,37,51] To confirm that the graphene surface is chemically functionalized successfully with PASE, we measure Raman spectra of the pristine and PASE-modified graphene (Figure S3c). There are two major peaks (the G and 2D peaks) in the spectrum of pristine graphene. Compared with the G peak, the strong and sharp 2D peak indicates the high quality and monolayer nature of graphene.[52] After conjugating PASE on the graphene surface, the D peak appears at about

https://doi.org/10.1021/jacs.1c06325
J. Am. Chem. Soc. 2021, 143, 17004−17014

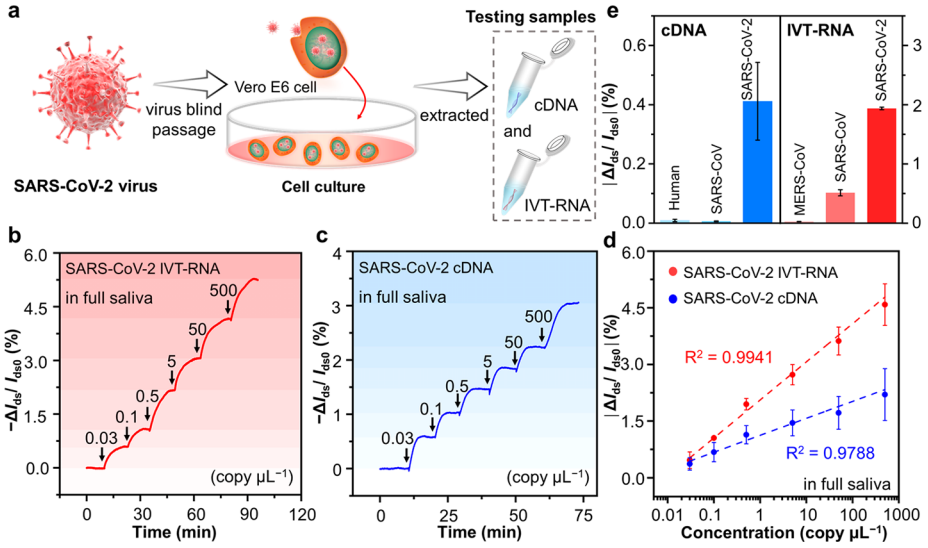

Figure 2. SARS-CoV-2 nucleic acid detection performance of the Y-dual probe g-FET biosensor. (a) Schematic diagram of SARS-CoV-2 nucleic acid sample preparation. (b, c) Real-time $\Delta I_{ds}/I_{ds0}$ response upon addition of SARS-CoV-2 IVT-RNA (b) and cDNA (c) solutions with different concentration (0.03 to 500 copy μL^{-1}) in full artificial saliva using the Y-dual probe g-FET biosensor. (d) Plots of $|\Delta I_{ds}/I_{ds0}|$ of the Y-dual probe g-FET biosensor versus SARS-CoV-2 IVT-RNA or cDNA concentration. (e) Selectivity of the Y-dual probe g-FET biosensor. $|\Delta I_{ds}/I_{ds0}|$ response upon addition of human cDNA (1 copy μL^{-1}), SARS-CoV cDNA (1 copy μL^{-1}), SARS-CoV-2 cDNA (0.1 copy μL^{-1}), MERS-CoV IVT-RNA (5 copy μL^{-1}), SARS-CoV IVT-RNA (5 copy μL^{-1}), and SARS-CoV-2 IVT-RNA (0.5 copy μL^{-1}). All the data points are obtained from three different devices.

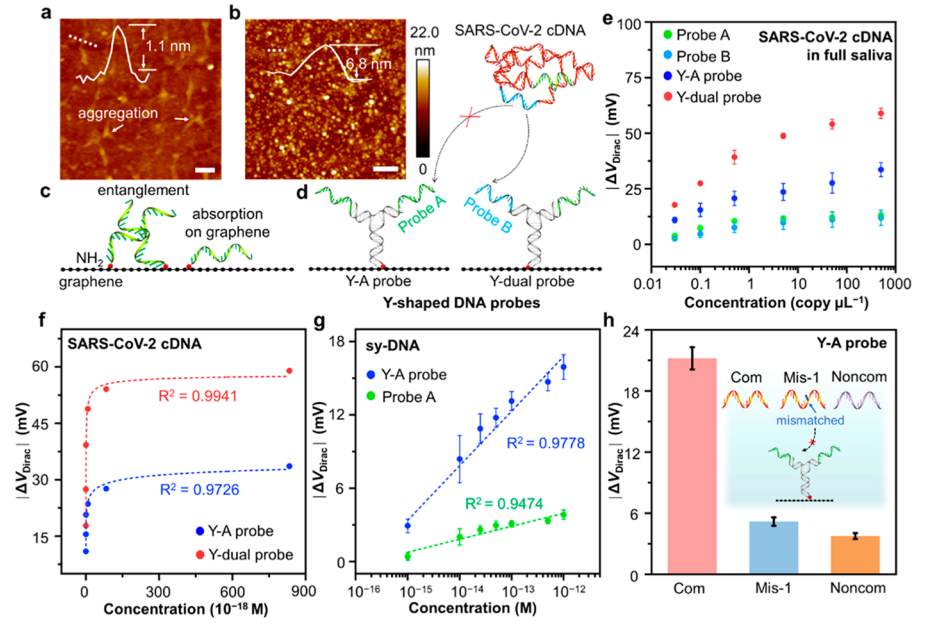

Figure 3. Performance comparison of Y-shaped DNA probe- and ss-DNA probe-modified g-FET biosensors. (a, b) AFM images (tapping mode in fluid) of graphene modified with ss-DNA probes (probe A) or Y-shaped DNA probes (Y-A probe). The scale bars are 150 and 300 nm. (c, d) Schematic illustration of the sensing interface of a g-FET biosensor modified with ss-DNA probes (c) or Y-shaped DNA probes (d). (e) ΔV_{Dirac} of a g-FET biosensor with different probes as a function of SARS-CoV-2 cDNA concentration from 0.03 to 500 copy μL^{-1} in 100 μL of full artificial saliva. (f) ΔV_{Dirac} versus SARS-CoV-2 cDNA concentration curves fitted by eq 1 for the Y-A probe and Y-dual probe, respectively. (g) ΔV_{Dirac} of g-FET biosensors as a function of sy-DNA concentration ranging from 1×10^{-15} to 1×10^{-12} M when using a Y-A probe or probe A in 0.01× PBS. (h) ΔV_{Dirac} of g-FET biosensors after exposure to target DNA sequences at a concentration of 1 μM for 30 min, demonstrating discrimination of sequences with single base-pair mismatches. All the data points are obtained from three different devices.

1350 cm^{-1}, and the D′ peak appears as the shoulder of the G peak, which prove the successful functionalization.[53,54] The mapping images show that the average I_{2D}/I_G ratio of PASE-modified graphene ($I_{2D}/I_G \approx 1.39$) is significantly lower than that of the pristine graphene ($I_{2D}/I_G \approx 2.57$), indicating the $\pi-\pi$ stacking of PASE on graphene (Figures S3d,e).[55]

The morphologies of the graphene before and after modifying PASE and Y-dual probes are characterized by atomic force microscopy in air (AFM, Figure S4). The pristine graphene has a flat surface with a height of 0.5−1 nm. The Y-dual probes when immobilized on the graphene surface have a height of 3.5−4 nm. To verify the modification, we design Y-

https://doi.org/10.1021/jacs.1c06325
J. Am. Chem. Soc. 2021, 143, 17004−17014

dual probes with the fluorescent dye cyanine 3 (Cy3) tethered to the 3′-terminal of the S2 sequence and anchor them on the graphene surface (Figure S5). In normal cases, the fluorescence will be quenched when the dyes are close to graphene.[56] The reason is that the nonradiative coupling between the emitter dipole and the electron−hole excitation in graphene leads to energy transfer.[57] Here, a significant fluorescence signal is observed (Figure 1e), indicating successful modification of the probes and the fact that the probes are upright at the interface without the conjugated dyes adsorbing on the graphene surface (see Supporting Information Section 1).

Real-Time Detection of SARS-CoV-2 Nucleic Acids. We evaluate the dynamic response of the Y-dual probe g-FET biosensors upon SARS-CoV-2 nucleic acids. Two samples (Figure 2a), SARS-CoV-2 in vitro-transcribed (IVT) RNA (containing OFR1ab, E and N gene) and SARS-CoV-2 virus extracted RNA reverse transcribed cDNA (cDNA, from a confirmed COVID-19 severe pneumonia case), are spiked in full artificial saliva to simulate the original environment. The probes (Table S1) targeting SARS-CoV-2 IVT-RNA or cDNA are functionalized on g-FET biosensors, respectively. Real-time current responses of g-FET biosensors immobilized with Y-dual probes (Figure 2b,c) are measured upon successive addition of SARS-CoV-2 IVT-RNA or cDNA with concentrations from 0.03 copy μL^{-1} (5.01×10^{-20} M) to 500 copy μL^{-1} (8.35×10^{-16} M). The current response is normalized as $\Delta I_{ds}/I_{ds0} = (I_{ds} - I_{ds0})/I_{ds0}$, where I_{ds} is the drain−source current and I_{ds0} is the initial value of I_{ds}. The response time, defined as the time when $\Delta I_{ds}/I_{ds0}$ reaches saturation, is as short as 4 min.

$|\Delta I_{ds}/I_{ds0}|$ of the g-FET biosensors follows a linear correlation with the target concentration in logarithmic scale (Figure 2d). The $|\Delta I_{ds}/I_{ds0}|$ responses upon 500 copy μL^{-1} SARS-CoV-2 IVT-RNA and cDNA are approximately 5.29% and 3.06%, respectively. The detectable concentration reaches 0.03 copy μL^{-1} for both targets, indicating ultrahigh sensitivity of the device. As a comparison, g-FET biosensors modified with ss-DNA probes (probe A or probe B) that can target SARS-CoV-2 IVT-RNA or cDNA have negligible $\Delta I_{ds}/I_{ds0}$ responses in full artificial saliva (Figure S6). Y-dual probe g-FET biosensors (Figure 2e, Figure S7) can distinguish SARS-CoV-2 nucleic acids with other nucleic acids (such as human cDNA, SARS-CoV cDNA, SARS-CoV IVT-RNA, and MERS-CoV IVT-RNA), showing high specificity in SARS-CoV-2 nucleic acid testing.

Detection Mechanism of the Y-Dual Probe g-FET Biosensor. Biodetection involves biorecognition and signal transduction processes.[38,46,48,58−60] Owing to the monolayer nature of graphene, all the charge carriers flow merely on the channel surface and are directly exposed to the external environment, ensuring highly efficient transduction and sensitive response to specific perturbations. On the other hand, the probe structure design is of great importance for the biorecognition (Figure 3). We prepare four DNA probe structures targeting SARS-CoV-2 cDNA to prove the structural superiority of the Y-dual probe, including probe A (targets ORF1ab gene, nt13377−13404), probe B (targets N gene, nt28934−28953), Y-A probe (two identical probe A are embedded), and Y-dual probe. In the cases of the Y-A probe and Y-dual probe (Figure S8a,b), Dirac points (V_{Dirac}, as the liquid-gate voltage (V_{lg}) when the drain−source current (I_{ds}) reaches its minimum) all remarkably shift toward negative V_{lg} with increasing concentration of cDNA, which indicates the n-type doping effect of graphene. This is attributed to the nonelectrostatic stacking interaction between graphene and electron-rich nuclear bases in cDNA molecules, which have been clearly studied theoretically and experimentally.[38,61,62] The g-FET biosensors (Figure S8c,d) with ss-DNA probes (probe A or probe B) have negligible shifts of V_{Dirac} (ΔV_{Dirac}). In particular, $|\Delta V_{Dirac}|$ of g-FET biosensors functionalized with a Y-dual probe reach up to 58.9 mV upon 500 copy μL^{-1} cDNA, around 2-fold larger than 33.6 mV of g-FET biosensors immobilized with a Y-A probe (Figure 3e).

The Y-shaped structure of the probe enables a higher biorecognition ratio compared with ss-DNA probes. The rigid stem structure of Y-shaped DNA probes can keep them upright at the interface and reduces the nonspecific adsorption of the probes on the graphene surface. AFM characterization shows the height of the immobilized probe A in fluid is about 1.1 nm, indicating that most of the ss-DNA probes are lying on the graphene surface (Figure 3a,c). In contrast, Y-A probes are uniformly anchored on the graphene surface with a height of ∼6.8 nm and a density of $\sim 4.32 \times 10^{9}$ cm^{-2} without aggregation (Figure 3b). The fluorescence experiment in Figure 1e is also in agreement with this result (see Supporting Information Section 1).

Moreover, the Y-shaped DNA probes have two recognition sites. The synergy effect of the two sites greatly enhance the hybridization ratio between probes and targets. To quantify the recognition ratio of the Y-shaped DNA probe and ss-DNA probe, we detect the synthetic DNA (sy-DNA, 28-mer, nt 13377−13404), a selective region of SARS-CoV-2 cDNA (Table S1), by g-FET biosensors immobilized with the Y-A probe (has two identical recognition sites) and probe A (has one recognition site), respectively. We measure transfer curves of g-FET biosensors upon addition of the sy-DNA with a concentration ranging from 1×10^{-15} to 1×10^{-12} M in 0.01× PBS (pH 7.2−7.4) (Figure S9). $|\Delta V_{Dirac}|$ shows a linear dependence upon the sy-DNA concentration in logarithmic scale (Figure 3g). The Y-A probe-modified g-FET biosensor produces a $|\Delta V_{Dirac}|$ response of ∼15.9 mV upon 1×10^{-12} M sy-DNA, while the $|\Delta V_{Dirac}|$ of the probe A-modified g-FET biosensor is ∼3.8 mV, indicating a 4.2-fold enhancement of the signal by using the Y-A probe. The assay sensitivity of the g-FET biosensor immobilized with the Y-A probe and probe A is $\sim 1.3 \times 10^{-4}$ and $\sim 3.4 \times 10^{-5}$ mV per decade of concentration, respectively. The change of charge carrier density (Δn) of graphene after adding sy-DNA molecules can be obtained from $\Delta V_{Dirac} = e\Delta n/C_{tot}$,[38,42] where C_{tot} is the total gate capacitance and e is the elementary charge. The Δn introduced by Y-A probes is estimated to be $\sim 2.51 \times 10^{12}$ cm^{-2} according to ΔV_{Dirac} before and after immobilizing Y-A probes (Figure S10). The hybridization ratio of Y-A probes to sy-DNA can also be calculated by Δn. When the concentration of sy-DNA is 1×10^{-15} M, the hybridization ratio is estimated to be ∼29.85% (Supporting Information Section 2).

The binding kinetics of DNA hybridization can be constrained by the Sips model,[37,63]

$$\Delta V_{Dirac} = \Delta V_{max} \frac{([A]/K_A)^n}{1 + ([A]/K_A)^n} \quad (1)$$

where ΔV_{max} is the ΔV_{Dirac} response with a maximum number of binding sites occupied, [A] is the concentration of the target, n represents a Gaussian distribution of DNA-binding energies, and K_A is the equilibrium dissociation constant

https://doi.org/10.1021/jacs.1c06325
J. Am. Chem. Soc. 2021, 143, 17004−17014

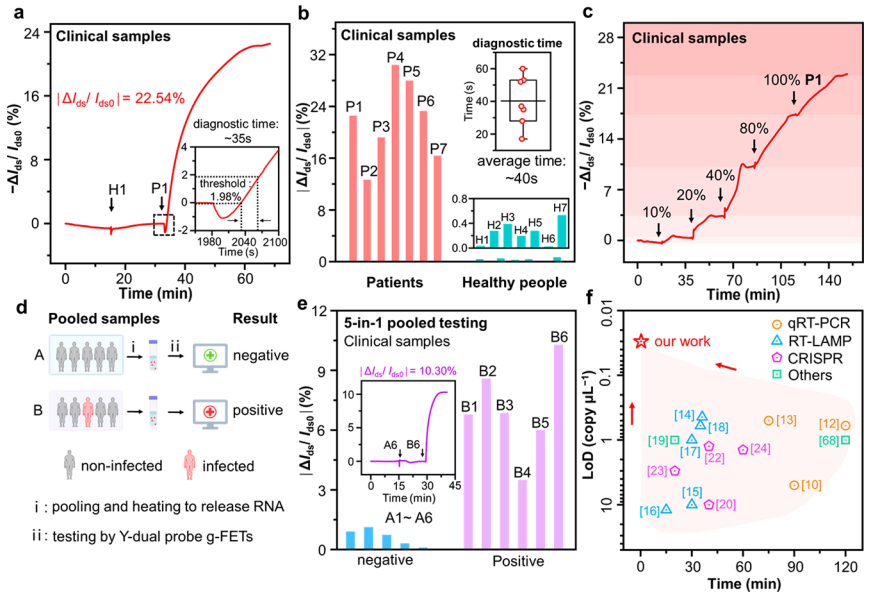

Figure 4. Unamplified and direct detection of SARS-CoV-2 clinical samples. (a) $\Delta I_{ds}/I_{ds0}$ versus time curve upon addition of healthy people sample H1 and clinical sample P1. Inset: Diagnostic time estimation for P1. (b) $\Delta I_{ds}/I_{ds0}$ upon addition of P1−P7 and H1−H7. Inset (up): Box plot of the diagnostic time for P1−P7. Inset (down): An enlarged view of $|\Delta I_{ds}/I_{ds0}|$ when H1−H7 are added. (c) Real-time $\Delta I_{ds}/I_{ds0}$ response of the g-FET biosensor upon various diluted concentrations of P1. (d) Workflows of 5-in-1 pooled testing of SARS-CoV-2 nucleic acid. (e) Real-time $|\Delta I_{ds}/I_{ds0}|$ response of Y-dual probe g-FET biosensors upon addition of positive samples B1−B6 and negative samples A1−A6. Inset: $|\Delta I_{ds}/I_{ds0}|$ versus time curve upon addition of pooled samples A6 and B6. (f) Performance comparison of the Y-dual probe g-FET biosensor with reported methods for SARS-CoV-2 nucleic acid detection.

values. The smaller the K_A value, the stronger the binding affinity.[64,65] K_A values can be estimated according to eq 1 by fitted curves. The estimated K_A of the Y-A probe is $(1.02 \pm 0.16) \times 10^{-14}$ M (Figure S11a). Since probe A has almost no offset when adding sy-DNA at a concentration of 10^{-12} M, we measure the responses of g-FET biosensors immobilized with probe A as a function of sy-DNA concentration ranging from 1×10^{-12} to 1×10^{-6} M (Figure S11b). K_A of probe A is estimated to be $(3.82 \pm 2.09) \times 10^{-11}$ M (Figure S11c). The lower K_A value of the Y-A probe compared with probe A indicates that the Y-shaped DNA probe improves the biorecognition ratio owing to more recognition sites. We measure the specificity of the biorecognition by using Y-A probes to detect complementary (Com, sy-DNA), single base-pair mismatch (Mis-1), and noncomplementary (Noncom) DNA sequences (Figure 3h). An appreciable ΔV_{Dirac} response up to ∼21.2 mV is observed for a Com DNA sequence (sy-DNA) at a concentration of 1 μM and a negligible ΔV_{Dirac} response smaller than 5.18 mV for Mis-1 and Noncom DNA sequences at the same concentration. Thus, the embedded sites of the Y-shaped DNA probes retain an upright orientation and remain active for specifically recognizing target sequences.

Due to complex secondary structures formed by the long sequence of SARS-CoV-2 nucleic acid, the Y-dual probe with two different probe sites targeting ORF1ab and N gene regions is able to enhance the recognition ratio toward real samples of viral nucleic acids (Figure 3d). According to eq 1, the fitted curves of ΔV_{Dirac} responses upon addition of SARS-CoV-2 cDNA (Figure 3f) yield $\Delta V_{max} = 39.8 \pm 8.6$ mV, $K_A = (1.37 \pm 2.89) \times 10^{-18}$ M, and $n = 0.23 \pm 0.09$ for the Y-A probe and $\Delta V_{max} = 53.2 \pm 2.9$ mV, $K_A = (0.083 \pm 0.026) \times 10^{-18}$ M, and $n = 0.97 \pm 0.37$ for the Y-dual probe. The larger ΔV_{max} of the Y-dual probe indicates more binding sites, while the smaller K_A suggests a decreased dissociation constant and increased binding affinity of the Y-dual probe. For further verification, the real-time $\Delta I_{ds}/I_{ds0}$ responses of the g-FET biosensor immobilized with the Y-A probe upon successive addition of SARS-CoV-2 cDNA with concentrations from 0.03 copy μL^{-1} (5.01×10^{-20} M) to 500 copy μL^{-1} (8.35×10^{-16} M) are shown in Figure S12. The response time is ∼7 min and $|\Delta I_{ds}/I_{ds0}|$ reaches ∼1.72% upon 500 copy μL^{-1} cDNA, which is about half of the Y-dual probe (∼3.06%, Figure 2c), indicating the binding ratio of the Y-dual probe with two different recognition sites is higher than that of the Y-A probe with two identical recognition sites.

Direct Testing of Clinical Samples. We test seven nasopharyngeal swab samples (P1−P7) collected from qRT-PCR-positive COVID-19 patients with Ct values ranging from 30.4 to 40.4 (Table S2) and seven samples (H1−H7) from healthy volunteers by Y-dual probe g-FET biosensors (Figure 4). All clinical samples are heated to release viral RNA and then tested directly without extraction. Y-dual probe g-FET biosensors correctly distinguish patient samples from healthy samples. $|\Delta I_{ds}/I_{ds0}|$ responses from P1 to P7 are larger than 12%, while negligible signals (<0.66%) are monitored for H1−H7 (Figure 4a,b, Figure S13). As a comparison, the pristine graphene device has a negligible response for H1 and P1 (Figure S14). We also demonstrate the specificity by detecting nonspecific proteins in full artificial saliva using g-FET biosensors immobilized with Y-dual probes. When 0.5 and 5 nM SARS-CoV-2 spike proteins are added sequentially, the g-FET biosensor had almost no response (Figure S15), indicating the specificity of the sensing interface against nonspecific proteins.

The $|\Delta I_{ds}/I_{ds0}|$ response is 0.81% upon 10% diluted P1 with a Ct value of 40.3 (Figure 4c), indicating the high sensitivity of the Y-dual probe g-FET biosensor in clinical detection. $I_{ds}-V_{lg}$ curves of g-FETs upon addition of diluted P2 show that the $\Delta I_{ds}/I_{ds0}$ versus time curves are measured in the p-type region (Figure S16). Consistent with the results of nonclinical

https://doi.org/10.1021/jacs.1c06325
J. Am. Chem. Soc. 2021, 143, 17004−17014

Table 1. Performance of Existing Methods for SARS-CoV-2 Nucleic Acid Testing

assay method	target	testing sample	LoD	amplification	time	ref
qRT-PCR (POC)	RdRp1/2, E, N and N1/2/3 gene	viral RNA	5 copy μL^{-1}	yes	<90 min	10
qRT-PCR (China NMPA)	ORF1ab and N gene	viral RNA	0.6−3.2 copy μL^{-1}	yes	>120 min	11
qRT-PCR (US CDC)	N1/2/3 gene	viral RNA	1−3.2 copy μL^{-1}	yes	>120 min	12
qRT-PCR	ORF1ab and N gene	ORF1ab and N gene cloned into plasmids	0.5 copy μL^{-1}	yes	75 min	13
RT-LAMP	S and E gene	viral RNA	0.44−1.09 copy μL^{-1}	yes	36 min	14
	ORF1ab gene	synthetic DNA	~10 copy μL^{-1}	yes	30−60 min	15
	ORF1ab gene	synthetic RNA	~12 copy μL^{-1}	yes	15−40 min	16
	ORF1ab, E and N gene	viral RNA	1 copy μL^{-1}	yes	30 min	17
	RdRp gene	viral RNA	0.6 copy μL^{-1}	yes	35−55 min	18
Exo-IQ-RT-RPA[a] assay	N gene	viral RNA	1 copy μL^{-1}	yes	20−25 min	19
RT-RAA[b]	S and ORF1ab gene	viral RNA	1 copy μL^{-1}	yes	20−25 min	20
Isothermal amplification	S gene	viral RNA	10 copy μL^{-1}	yes	60 min	21
CRISPR	E and N gene	synthetic RNA	10 copy μL^{-1}	yes	40 min	22
	ORF1ab gene	viral RNA	1.25 copy μL^{-1}	yes	40 min	23
	N gene	viral RNA	3 copy μL^{-1}	yes	20 min	24
	S, N and ORF1ab gene	viral RNA	1.42 copy μL^{-1}	yes	>60 min	25
	ORF1ab and E gene	IVT-RNA fragment	3×10^8 copy μL^{-1}	no	>60 min	69
electrochemical assay	S and N gene	viral RNA	1 copy μL^{-1}	yes	<120 min	70
Y dual-probe g-FET biosensor	ORF1ab and N gene	viral RNA	0.03 copy μL^{-1}	no	0.7 min	this work

[a]Exoprobe with an internally linked quencher reverse transcription recombinase polymerase amplification. [b]Reverse transcription recombinase-aided amplification.

samples testing, we also observed that V_{Dirac} remarkably shifts toward negative V_{lg} with increasing diluted concentrations of P2, indicating the n-type doping effects on graphene. The diagnostic time is read from the interception of the threshold value and the real-time ΔI_{ds} responses. The threshold value to diagnose COVID-19 by Y-dual probe g-FET biosensors is taken from 3 times the largest $|\Delta I_{ds}/I_{ds0}|$ response of the negative samples. In the COVID-19 individual testing (P1−P7), the largest $|\Delta I_{ds}/I_{ds0}|$ response of H1−H7 is around 0.66%, and thus the threshold value is set to be 1.98%. The diagnostic time is 0.3−1 min for P1−P7 with an average of ~40 s (Figure 4b, Figure S13).

Direct 5-in-1 Pooled Testing. Some reports have verified the feasibility of pooling samples for qRT-PCR testing in COVID-19 screening.[30,31] The pooled testing has been successfully used in Israel during the COVID-19 pandemic to process ~133 000 samples over a period of variable prevalence, leading to resource savings.[66] To demonstrate the application potential of Y-dual probe g-FET biosensors in large-scale screening, we conduct 5-in-1 pooled testing of SARS-CoV-2 nucleic acid (Figure 4d). Five nasopharyngeal swab samples are mixed, heat treated, and detected together by Y-dual probe g-FET biosensors. The pooled samples (A1−A6, obtained by pooling 5 negative samples) have a negligible $|\Delta I_{ds}/I_{ds0}|$ response smaller than 1.13% (Figure 4e, Figure S17), while other pooled samples (B1−B6, obtained by pooling 4 negative samples and 1 positive sample) have responses between 3.51% and 8.59%, in agreement with the qRT-PCR results. Considering the dilution of the infected specimen(s) and high complexity of the composition,[30] the accurate pooled testing indicates the ultrasensitive feature of the Y-dual probe g-FET biosensors. The largest $|\Delta I_{ds}/I_{ds0}|$ response of A1−A6 is about 1.32%, so the threshold value is 3.96%. The diagnostic time for 5-in-1 pooled sample B6 is within 1 min (Figure S18). The pooled testing by Y-dual probe g-FET biosensors avoids complicated and long-time amplification processes, with great potential for efficient population screening.

CONCLUSIONS

In this article, we report a direct SARS-CoV-2 nucleic acid testing methodology based on Y-dual probe g-FET biosensors and address an urgent issue of COVID-19 testing that faces a trade-off between accuracy and speed of report. Compared with other methods,[10−25,67,68] The Y-dual probe g-FET biosensor has excellent performance in terms of diagnostic time and LoD (Figure 4f, Table 1). The diagnostic time (0.3−1 min) is comparable to serological tests (0.2−15 min) and faster than existing nucleic acid testing technologies such as RT-LAMP (15−60 min), CRISPR (>20 min), electrochemistry (<120 min), qRT-PCR and commercial kits (25−420 min), etc. Although the samples are unamplified, the LoD still reaches 0.03 copy μL^{-1}, at least 20-fold lower than the U.S. Centers for Disease Control and Prevention (CDC)/China National Medical Products Administration (NMPA)-approved qRT-PCR assays (0.6−3.2 copies μL^{-1}).[11,12] It is known that the viral load in the specimen is low in the early or late stages of infected COVID-19[50,68] and varies with specimen types, collection methods, and time of collection, which easily cause false-negative results.[69,70] The high sensitivity of Y dual-probe g-FET biosensors will be beneficial to ensure the testing accuracy for samples with a low viral load.

Viral RNA isolation from clinical samples as well as subsequent purification and amplification require trained personnel and specialized tools, leading to shortcomings in cost, diagnostic time, laborious processes, etc.[71] In epidemic control and prevention for highly infectious diseases such as COVID-19, speed and frequency of the screening tests, to a certain degree, matter more than accuracy. The Y-dual probe g-FET biosensors omit the time-consuming and complicated

https://doi.org/10.1021/jacs.1c06325
J. Am. Chem. Soc. 2021, 143, 17004−17014

processes for nucleic acid extraction and amplification and quickly obtain the results. More importantly, the Y-dual probe g-FET biosensors also perform well in pooled testing. In screening, pooled testing is an effective strategy to increase testing throughput, limit the use of reagents, and improve overall testing efficiency.[70] However, due to the dilution of samples, the pooled testing may miss individuals in whom COVID-19 risk has not been identified.[72] The specimens most likely to be lost due to dilution are those samples with low viral loads near the LoD of qRT-PCR. Here, the ultralow LoD of Y-dual probe g-FET biosensors enables pooled testing with high accuracy even though the samples are unamplified.

By integrating with a portable microelectronic system, on-site and point-of-care (POC) COVID-19 tests can be achieved at airports, rail stations, local clinics, and even at home. Considering the advantages such as quick diagnoses, high sensitivity, easy operation, low cost, portability, and integration, the Y-dual probe g-FET biosensor can be applied for COVID-19 screening in places where an outbreak has occurred. Apart from SARS-CoV-2, by replacing the probes, ultraprecise diagnostics of other infectious diseases in a few minutes is expected in the future. As such, the Y-dual probe g-FET biosensor can be a comprehensive testing method with potential in precise diagnostics and wide-population screening of COVID-19 and other pandemics.

METHODS

Synthesis of a Y-Shaped DNA Probe. All oligonucleotide sequences used in the experiment (Table S1) were prepared and purified by Sangon Biotechnology Inc. Oligonucleotides used to assemble the Y-shaped DNA probes were dissolved in TE buffer (10 mM Tris HCL, 1 mM EDTA, pH ~8.0) at a final concentration of 1 μM for each strand. The mixed DNA strands were hybridized by a thermal cycler (SimpliAmp, Thermo Fisher Scientific) following the listed procedures:[73,74] (i) denatured at 95 °C for 2 min; (ii) cooled to 65 °C and incubated for 5 min; (iii) annealed at 60 °C for 2 min; (iv) decreasing the temperature from 60 °C at a rate of 0.1 °C every 30 s until it reached 55 °C; this process was repeated 40 times in total. The final product was stored at 4 °C.

Fabrication of the g-FET Biosensor. Monolayer graphene was prepared in a tube furnace (GSL 1200X) via chemical vapor deposition on a 25 μm thick Cu foil according to the method reported previously.[52] The graphene grown on the Cu foil was transferred by poly(methyl methacrylate) (PMMA) to the SiO_2/Si substrate by an electrochemical bubbling method. The g-FET biosensors were fabricated via a thermally assisted bilayer lift-off photolithography process (Microwriter ML3, Durham Magneto Optics Ltd.), with Cr/Au (5/40 nm) electrodes deposited by thermal evaporator (Angstrom Engineering). The transferred graphene was patterned via standard photolithography and etching techniques to define the channel region. To functionalize the Y-dual probes on the graphene surface, the g-FET biosensors were immersed in a dimethyl sulfoxide (DMSO, Sigma-Aldrich) solution of 5 mM PASE (Sigma-Aldrich) for 2 h at room temperature. After thoroughly rinsing by ethanol and deionized water, the sensors were incubated in a solution of 1 μM Y-shaped DNA probe solution for 12 h. After incubation, 100 mM ethanolamine was added for 1 h to inactivate and block the excess reactive groups remaining on the graphene surface.

Characterization. The graphene was characterized by TEM (Tecnai G2 F20 S-Twin, acceleration voltage: 200 kV). The graphene surfaces before and after PASE modification were measured by Raman spectrometer (LabRam HR Evolution, Horiba Jobin Yvon, 532 nm Ar ion laser). The formation of Y-dual probes was analyzed using 10% native polyacrylamide gel electrophoresis (Acr/Bis = 29:1; Acr = acrylamide, Bis = *N*,*N*′-methylene bis(acrylamide)) in 1× TAE Mg^{2+} buffer (2 M Tris-acetate,1 mM EDTA, 12.5 mM Mg^{2+}, pH ~8.0) at 90 V for 90 min, and then the gels were stained in Sybr Safe (Thermo Fisher) for 30 min followed by imaging under UV exposure (Gel-doc XR+, Biorad). The suface morphology of graphene after each functionalization step was imaged by AFM (Fastscan, Bruke), under tapping mode in air with a 20−25 nm radius tip (Scanasyst air, Bruker). The g-FET biosensors modified with ss-DNA probes (probe A) and Y-A probes were analyzed in TE buffer by AFM (Fastscan, Bruke) under ScanAsyst mode using an ultrasharp tip (Fluid+, Bruke) of 2−3 nm radius.

Confocal Fluorescence Microscopy Measurement. The Cy3-conjugated S2 oligonucleotide strand and two other unfunctionalized oligonucleotides were mixed in a 1:1:1 ratio in TE buffer to synthesize Cy3-conjugated Y-dual probes. Graphene was transferred onto a quartz substrate with prepatterned gold electrodes and patterns, then modified with the Cy3-conjugated Y-dual probes. The g-FET biosensor was incubated in a solution of Y-dual probes tagged with Cy3 for 12 h, and then the graphene surface was rinsed using TE buffer. Finally, the fluorescence was imaged by confocal fluorescence microscope (C2+, Nikon) in TE buffer.

Cells and Virus. The SARS-CoV-2 strain nCoV-SH01 (GenBank: MT121215.1) from a laboratory-confirmed COVID-19 severe pneumonia case provided by CDC Shanghai was propagated in African green monkey kidney cell line Vero E6 cells (Cell Bank of Chinese Academy of Sciences, Shanghai, China). Vero E6 cells and human kidney cells HEK293 were cultured under a humidified atmosphere of 5% CO_2 at 37 °C in Dulbecco's modified Eagle medium (Gibco, Carlsbad, CA, USA), which contained 1% (v/v) penicillin, 2 mM L-glutamine, 100 mg mL^{-1} streptomycin, and 10% (v/v) fetal bovine serum (Gibco).

Preparation of Test Samples. SARS-CoV-2 cDNA and human cDNA were extracted from Vero E6 and HEK293 cells by using TRIzol reagent (Invitrogen, Carlsbad, CA, USA) and SuperScript III CellsDirect cDNA synthesis kit (Invitrogen) following the manufacturer's instructions. SARS-CoV-2, SARS-CoV, and MERS-CoV IVT-RNA reference materials (nt 13321−15540, GenBank No. MT027064.1, No. NC004718.3, and No. NC019843.3) containing N, E, and ORF1ab gene sequences with a titer of 10^5 copy μL^{-1} were provided from Shanghai Institute of Measurement and Testing Technology (SIMT). All samples were centrifuged at 3000 rpm at 4 °C for 5 min and then diluted in full artificial saliva (pH 6.8, Solarbio, China) and 2% RNase inhibitor (Thermo Fisher) to a test concentrations of 500, 50, 5, 0.5, 0.1, and 0.03 copy μL^{-1}. SARS-CoV-2 spike protein (40591-V08H, Sino Biological, Inc., China) was added into full artificial saliva to prepare control samples.

Clinical Samples. Seven nasopharyngeal swab samples from qRT-PCR-positive COVID-19 patients were collected from Department of Laboratory Medicine, Shanghai Public Health Clinical Center. The other seven nasopharyngeal swab samples were from healthy volunteers. The 5-in-1 pooled samples (B1−B7) by mixing non-infected pooled nasopharyngeal swab samples from four healthy volunteers with qRT-PCR confirmed COVID-19 samples P1−P4, P6, and P7 respectively. Pooled samples A1−A7 were obtained from nasopharyngeal swabs of five healthy volunteers. Without an extraction procedure, 200 μL of viral transport medium (Yocon, China) used to store the swab was heated at 56 °C for 30 min to release the RNA of all nasopharyngeal swab samples. Then, the medium was directly used for SARS-CoV-2 nucleic acid testing by Y-dual probe g-FETs. This research was approved by the Shanghai Public Health Clinical Center Ethics Committee (approval ID number: 2020-Y114-01) with informed consent from participants.

Device Measurement. The electrical characterization of g-FETs was carried out in ambient conditions using a semiconductor analyzer (Keysight, B1500A). A PDMS well with a volume of ~100 μL was placed on the graphene sensing region to hold testing solutions. To measure the $I_{ds}-V_{lg}$ curve of g-FET biosensors, a Ag/AgCl reference electrode was injected, the V_{lg} was swept from −0.4 to 0.6 V, and the Dirac point (V_{Dirac}) was obtained at a V_{lg} where I_{ds} reached its minimum. For the real-time ΔI_{ds} measurement, a drain−source bias (V_{ds}) of 50 mV was applied, and the I_{ds} was recorded throughout the experiments at a certain V_{lg}.

https://doi.org/10.1021/jacs.1c06325
J. Am. Chem. Soc. 2021, 143, 17004−17014

To measure analytes by g-FET biosensors, the sensor was first immersed in 100 μL of buffer solution or full artificial saliva, and then a stable V_{ds} bias was applied between the drain and source electrodes. After the I_{ds} stabilized, time-resolved I_{ds} measurement was performed. To add the testing solutions, a 10% volume solution was taken out from the PDMS well and replaced by 10 μL of premixed testing solutions. At the same time, real-time I_{ds} curves were recorded. To test clinical samples, we first immersed the g-FET biosensors in 100 μL of viral transport medium (VTM), and then a stable V_{ds} bias (50 mV) was applied between the drain and the source electrodes. After the I_{ds} stabilized, we took out 100 μL of VTM from the PDMS well and then added 100 μL of healthy samples (Hi). After the I_{ds} stabilized, we took out 100 μL of Hi and added 100 μL of the samples from COVID-19 patients.

■ ASSOCIATED CONTENT

Supporting Information

The Supporting Information is available free of charge at https://pubs.acs.org/doi/10.1021/jacs.1c06325.

Cy3 fluorescence on graphene, calculation of hybridization ratio, supplementary figures (Figures S1−S18), supplementary tables (Table S1 and S2) (PDF)

■ AUTHOR INFORMATION

Corresponding Author

Dacheng Wei − *State Key Laboratory of Molecular Engineering of Polymers, Department of Macromolecular Science and Institute of Molecular Materials and Devices, Fudan University, Shanghai 200433, China;* orcid.org/0000-0003-3593-9897; Email: weidc@fudan.edu.cn

Authors

Derong Kong − *State Key Laboratory of Molecular Engineering of Polymers, Department of Macromolecular Science and Institute of Molecular Materials and Devices, Fudan University, Shanghai 200433, China*

Xuejun Wang − *State Key Laboratory of Molecular Engineering of Polymers, Department of Macromolecular Science and Institute of Molecular Materials and Devices, Fudan University, Shanghai 200433, China;* orcid.org/0000-0002-7034-0460

Chenjian Gu − *Key Laboratory of Medical Molecular Virology (MOE/NHC/CAMS), Department of Medical Microbiology and Parasitology, School of Basic Medical Sciences, Shanghai Medical College, Fudan University, Shanghai 200433, China*

Mingquan Guo − *Department of Laboratory Medicine, Shanghai Public Health Clinical Center, Fudan University, Shanghai 201508, China*

Yao Wang − *Key Laboratory of Medical Molecular Virology (MOE/NHC/CAMS), Department of Medical Microbiology and Parasitology, School of Basic Medical Sciences, Shanghai Medical College, Fudan University, Shanghai 200433, China*

Zhaolin Ai − *State Key Laboratory of Molecular Engineering of Polymers, Department of Macromolecular Science and Institute of Molecular Materials and Devices, Fudan University, Shanghai 200433, China*

Shen Zhang − *State Key Laboratory of Molecular Engineering of Polymers, Department of Macromolecular Science and Institute of Molecular Materials and Devices, Fudan University, Shanghai 200433, China*

Yiheng Chen − *State Key Laboratory of Molecular Engineering of Polymers, Department of Macromolecular Science and Institute of Molecular Materials and Devices, Fudan University, Shanghai 200433, China*

Wentao Liu − *State Key Laboratory of Molecular Engineering of Polymers, Department of Macromolecular Science and Institute of Molecular Materials and Devices, Fudan University, Shanghai 200433, China*

Yungen Wu − *State Key Laboratory of Molecular Engineering of Polymers, Department of Macromolecular Science and Institute of Molecular Materials and Devices, Fudan University, Shanghai 200433, China*

Changhao Dai − *State Key Laboratory of Molecular Engineering of Polymers, Department of Macromolecular Science and Institute of Molecular Materials and Devices, Fudan University, Shanghai 200433, China*

Qianying Guo − *State Key Laboratory of Molecular Engineering of Polymers, Department of Macromolecular Science and Institute of Molecular Materials and Devices, Fudan University, Shanghai 200433, China*

Di Qu − *Key Laboratory of Medical Molecular Virology (MOE/NHC/CAMS), Department of Medical Microbiology and Parasitology, School of Basic Medical Sciences, Shanghai Medical College, Fudan University, Shanghai 200433, China*

Zhaoqin Zhu − *Department of Laboratory Medicine, Shanghai Public Health Clinical Center, Fudan University, Shanghai 201508, China*

Youhua Xie − *Key Laboratory of Medical Molecular Virology (MOE/NHC/CAMS), Department of Medical Microbiology and Parasitology, School of Basic Medical Sciences, Shanghai Medical College, Fudan University, Shanghai 200433, China*

Yunqi Liu − *Institute of Molecular Materials and Devices, Fudan University, Shanghai 200433, China; Institute of Chemistry, Chinese Academy of Sciences, Beijing 100190, China;* orcid.org/0000-0001-5521-2316

Complete contact information is available at: https://pubs.acs.org/10.1021/jacs.1c06325

Author Contributions

The manuscript was written through contributions of all authors. All authors have given approval to the final version of the manuscript.

Notes

The authors declare no competing financial interest.

■ ACKNOWLEDGMENTS

This work was supported by the National Key R&D Program of China (2021YFE0201400), National Natural Science Foundation of China (51773041, 61890940), the Strategic Priority Research Program of the Chinese Academy of Sciences (XDB30000000), China Postdoctoral Science Foundation (2019M661353), National Postdoctoral Program for Innovative Talents (BX20190072), Chongqing Bayu Scholar Program (DP2020036), and Fudan University.

■ REFERENCES

(1) Du Toit, A. Getting carried away. *Nat. Rev. Microbiol.* **2020**, *18*, 122−123.

(2) Yuan, X.; Yang, C.; He, Q.; Chen, J.; Yu, D.; Li, J.; Zhai, S.; Qin, Z.; Du, K.; Chu, Z.; Qin, P. Current and Perspective Diagnostic Techniques for COVID-19. *ACS Infect. Dis.* **2020**, *6* (8), 1998−2016.

(3) Lu, R.; Zhao, X.; Li, J.; Niu, P.; Yang, B.; Wu, H.; Wang, W.; Song, H.; Huang, B.; Zhu, N.; Bi, Y.; Ma, X.; Zhan, F.; Wang, L.; Hu, T.; Zhou, H.; Hu, Z.; Zhou, W.; Zhao, L.; Chen, J.; Meng, Y.; Wang, J.; Lin, Y.; Yuan, J.; Xie, Z.; Ma, J.; Liu, W. J.; Wang, D.; Xu, W.; Holmes, E. C.; Gao, G. F.; Wu, G.; Chen, W.; Shi, W.; Tan, W. Genomic characterisation and epidemiology of 2019 novel

coronavirus: implications for virus origins and receptor binding. *Lancet* **2020**, *395* (10224), 565−574.
(4) Weissleder, R.; Lee, H.; Ko, J.; Pittet, M. J. COVID-19 diagnostics in context. *Sci. Transl. Med.* **2020**, *12* (546), eabc1931.
(5) Li, R.; Pei, S.; Chen, B.; Song, Y.; Zhang, T.; Yang, W.; Shaman, J. Substantial undocumented infection facilitates the rapid dissemination of novel coronavirus (SARS-CoV-2). *Science* **2020**, *368* (6490), 489−493.
(6) He, X.; Lau, E. H. Y.; Wu, P.; Deng, X.; Wang, J.; Hao, X.; Lau, Y. C.; Wong, J. Y.; Guan, Y.; Tan, X.; Mo, X.; Chen, Y.; Liao, B.; Chen, W.; Hu, F.; Zhang, Q.; Zhong, M.; Wu, Y.; Zhao, L.; Zhang, F.; Cowling, B. J.; Li, F.; Leung, G. M. Temporal dynamics in viral shedding and transmissibility of COVID-19. *Nat. Med.* **2020**, *26* (5), 672−675.
(7) Service, R. F. Fast, cheap tests could enable safer reopening. *Science* **2020**, *369* (6504), 608−609.
(8) Yousefi, H.; Mahmud, A.; Chang, D.; Das, J.; Gomis, S.; Chen, J. B.; Wang, H.; Been, T.; Yip, L.; Coomes, E.; Li, Z.; Mubareka, S.; McGeer, A.; Christie, N.; Gray-Owen, S.; Cochrane, A.; Rini, J. M.; Sargent, E. H.; Kelley, S. O. Detection of SARS-CoV-2 Viral Particles Using Direct, Reagent-Free Electrochemical Sensing. *J. Am. Chem. Soc.* **2021**, *143* (4), 1722−1727.
(9) Deng, J.; Tian, F.; Liu, C.; Liu, Y.; Zhao, S.; Fu, T.; Sun, J.; Tan, W. Rapid One-Step Detection of Viral Particles Using an Aptamer-Based Thermophoretic Assay. *J. Am. Chem. Soc.* **2021**, *143* (19), 7261−7266.
(10) Gibani, M. M.; Toumazou, C.; Sohbati, M.; Sahoo, R.; Karvela, M.; Hon, T. K.; De Mateo, S.; Burdett, A.; Leung, K. Y. F.; Barnett, J.; Orbeladze, A.; Luan, S.; Pournias, S.; Sun, J.; Flower, B.; Bedzo-Nutakor, J.; Amran, M.; Quinlan, R.; Skolimowska, K.; Herrera, C.; Rowan, A.; Badhan, A.; Klaber, R.; Davies, G.; Muir, D.; Randell, P.; Crook, D.; Taylor, G. P.; Barclay, W.; Mughal, N.; Moore, L. S. P.; Jeffery, K.; Cooke, G. S. Assessing a novel, lab-free, point-of-care test for SARS-CoV-2 (CovidNudge): a diagnostic accuracy study. *Lancet Microbe* **2020**, *1* (7), e300−e307.
(11) China National Center for Clinical Laboratories. *Validation Report of real-time RT-PCR panel for detection 2019-nCoV*. https://www.nccl.org.cn/mainEn (accessed June 17, 2021).
(12) CDC. *CDC 2019-Novel Coronavirus (2019-nCoV) Real-Time RT-PCR Diagnostic Panel*. https://www.fda.gov/media/134922/download (accessed June 18, 2021).
(13) Chu, D. K. W.; Pan, Y.; Cheng, S. M. S.; Hui, K. P. Y.; Krishnan, P.; Liu, Y.; Ng, D. Y. M.; Wan, C. K. C.; Yang, P.; Wang, Q.; Peiris, M.; Poon, L. L. M. Molecular Diagnosis of a Novel Coronavirus (2019-nCoV) Causing an Outbreak of Pneumonia. *Clin. Chem.* **2020**, *66* (4), 549−555.
(14) Xun, G.; Lane, S. T.; Petrov, V. A.; Pepa, B. E.; Zhao, H. A rapid, accurate, scalable, and portable testing system for COVID-19 diagnosis. *Nat. Commun.* **2021**, *12* (1), 2905.
(15) Lamb, L. E.; Bartolone, S. N.; Ward, E.; Chancellor, M. B. Rapid detection of novel coronavirus/Severe Acute Respiratory Syndrome Coronavirus 2 (SARS-CoV-2) by reverse transcription-loop-mediated isothermal amplification. *PLoS One* **2020**, *15* (6), e0234682.
(16) Yu, L.; Wu, S.; Hao, X.; Dong, X.; Mao, L.; Pelechano, V.; Chen, W. H.; Yin, X. Rapid detection of COVID-19 coronavirus using a reverse transcriptional loop-mediated isothermal amplification (RT-LAMP) diagnostic platform. *Clin. Chem.* **2020**, *66* (7), 975−977.
(17) Yang, W.; Dang, X.; Wang, Q.; Xu, M.; Zhao, Q.; Zhou, Y.; Zhao, H.; Wang, L.; Xu, Y.; Wang, J.; Han, S.; Wang, M.; Pei, F.; Wan, Y. Rapid detection of SARS-CoV-2 using reverse transcription RT-LAMP method. *medRxiv* **2020**, DOI: 10.1101/2020.03.02.20030130, (accessed on June 18, 2021).
(18) Woo, C. H.; Jang, S.; Shin, G.; Jung, G. Y.; Lee, J. W. Sensitive fluorescence detection of SARS-CoV-2 RNA in clinical samples via one-pot isothermal ligation and transcription. *Nat. Biomed. Eng.* **2020**, *4* (12), 1168−1179.
(19) Behrmann, O.; Bachmann, I.; Spiegel, M.; Schramm, M.; Abd El Wahed, A.; Dobler, G.; Dame, G.; Hufert, F. T. Rapid detection of SARS-CoV-2 by low volume real-time single tube reverse transcription recombinase polymerase amplification using an exo probe with an internally linked quencher (Exo-IQ). *Clin. Chem.* **2020**, *66* (8), 1047−1054.
(20) Xue, G.; Li, S.; Zhang, W.; Du, B.; Cui, J.; Yan, C.; Huang, L.; Chen, L.; Zhao, L.; Sun, Y.; Li, N.; Zhao, H.; Feng, Y.; Wang, Z.; Liu, S.; Zhang, Q.; Xie, X.; Liu, D.; Yao, H.; Yuan, J. Reverse-transcription recombinase-aided amplification assay for rapid detection of the 2019 novel coronavirus (SARS-CoV-2). *Anal. Chem.* **2020**, *92* (14), 9699−9705.
(21) Broughton, J. P.; Deng, X.; Yu, G.; Fasching, C. L.; Servellita, V.; Singh, J.; Miao, X.; Streithorst, J. A.; Granados, A.; Sotomayor-Gonzalez, A.; Zorn, K.; Gopez, A.; Hsu, E.; Gu, W.; Miller, S.; Pan, C. Y.; Guevara, H.; Wadford, D. A.; Chen, J. S.; Chiu, C. Y. CRISPR-Cas12-based detection of SARS-CoV-2. *Nat. Biotechnol.* **2020**, *38* (7), 870−874.
(22) Yang, K.; Chaput, J. C. REVEALR: A multicomponent XNAzyme-based nucleic acid detection system for SARS-CoV-2. *J. Am. Chem. Soc.* **2021**, *143* (24), 8957−8961.
(23) Hou, T.; Zeng, W.; Yang, M.; Chen, W.; Ren, L.; Ai, J.; Wu, J.; Liao, Y.; Gou, X.; Li, Y.; Wang, X.; Su, H.; Gu, B.; Wang, J.; Xu, T. Development and evaluation of a rapid CRISPR-based diagnostic for COVID-19. *PLoS Pathog.* **2020**, *16* (8), e1008705.
(24) Ding, X.; Yin, K.; Li, Z.; Lalla, R. V.; Ballesteros, E.; Sfeir, M. M.; Liu, C. Ultrasensitive and visual detection of SARS-CoV-2 using all-in-one dual CRISPR-Cas12a assay. *Nat. Commun.* **2020**, *11* (1), 4711.
(25) Patchsung, M.; Jantarug, K.; Pattama, A.; Aphicho, K.; Suraritdechachai, S.; Meesawat, P.; Sappakhaw, K.; Leelahakorn, N.; Ruenkam, T.; Wongsatit, T.; Athipanyasilp, N.; Eiamthong, B.; Lakkanasirorat, B.; Phoodokmai, T.; Niljianskul, N.; Pakotiprapha, D.; Chanarat, S.; Homchan, A.; Tinikul, R.; Kamutira, P.; Phiwkaow, K.; Soithongcharoen, S.; Kantiwiriyawanitch, C.; Pongsupasa, V.; Trisrivirat, D.; Jaroensuk, J.; Wongnate, T.; Maenpuen, S.; Chaiyen, P.; Kamnerdnakta, S.; Swangsri, J.; Chuthapisith, S.; Sirivatanauksorn, Y.; Chaimayo, C.; Sutthent, R.; Kantakamalakul, W.; Joung, J.; Ladha, A.; Jin, X.; Gootenberg, J. S.; Abudayyeh, O. O.; Zhang, F.; Horthongkham, N.; Uttamapinant, C. Clinical validation of a Cas13-based assay for the detection of SARS-CoV-2 RNA. *Nat. Biomed. Eng.* **2020**, *4* (12), 1140−1149.
(26) Chan, J. F.; Yuan, S.; Kok, K. H.; To, K. K.; Chu, H.; Yang, J.; Xing, F.; Liu, J.; Yip, C. C.; Poon, R. W.; Tsoi, H. W.; Lo, S. K.; Chan, K. H.; Poon, V. K.; Chan, W. M.; Ip, J. D.; Cai, J. P.; Cheng, V. C.; Chen, H.; Hui, C. K.; Yuen, K. Y. A familial cluster of pneumonia associated with the 2019 novel coronavirus indicating person-to-person transmission: a study of a family cluster. *Lancet* **2020**, *95* (10223), 514−523.
(27) Pan, Y.; Zhang, D.; Yang, P.; Poon, L. L. M.; Wang, Q. Viral load of SARS-CoV-2 in clinical samples. *Lancet Infect. Dis.* **2020**, *20* (4), 411−412.
(28) Mina, M. J.; Andersen, K. G. COVID-19 testing: One size does not fit all. *Science* **2021**, *371* (6525), 126−127.
(29) Centers for Disease Control and Prevention. *Overview of testing for SARS-CoV-2 (COVID-19)*. https://www.cdc.gov/coronavirus/2019-ncov/hcp/testing-overview.html (accessed June 18, 2021).
(30) Mutesa, L.; Ndishimye, P.; Butera, Y.; Souopgui, J.; Uwineza, A.; Rutayisire, R.; Ndoricimpaye, E. L.; Musoni, E.; Rujeni, N.; Nyatanyi, T.; Ntagwabira, E.; Semakula, M.; Musanabaganwa, C.; Nyamwasa, D.; Ndashimye, M.; Ujeneza, E.; Mwikarago, I. E.; Muvunyi, C. M.; Mazarati, J. B.; Nsanzimana, S.; Turok, N.; Ndifon, W. A pooled testing strategy for identifying SARS-CoV-2 at low prevalence. *Nature* **2021**, *589* (7841), 276−280.
(31) Cleary, B.; Hay, J. A.; Blumenstiel, B.; Harden, M.; Cipicchio, M.; Bezney, J.; Simonton, B.; Hong, D.; Senghore, M.; Sesay, A. K.; Gabriel, S.; Regev, A.; Mina, M. J. Using viral load and epidemic dynamics to optimize pooled testing in resource-constrained settings. *Sci. Transl. Med.* **2021**, *13* (589), eabf1568.

(32) Zhang, X.; Jing, Q.; Ao, S.; Schneider, G. F.; Kireev, D.; Zhang, Z.; Fu, W. Ultrasensitive field-effect biosensors enabled by the unique electronic properties of graphene. *Small* **2020**, *16* (15), e1902820.
(33) Sadighbayan, D.; Hasanzadeh, M.; Ghafar-Zadeh, E. Biosensing based on field-effect transistors (FET): Recent progress and challenges. *TrAC, Trends Anal. Chem.* **2020**, *133*, 116067.
(34) Kim, J.; Campbell, A. S.; de Ávila, B. E.; Wang, J. Wearable biosensors for healthcare monitoring. *Nat. Biotechnol.* **2019**, *37* (4), 389−406.
(35) Flampouri, E.; Imar, S.; O Connell, K.; Singh, B. Spheroid-3D and monolayer-2D intestinal electrochemical biosensor for toxicity/viability testing: applications in drug screening, food safety, and environmental pollutant analysis. *ACS Sens.* **2019**, *4* (3), 660−669.
(36) Xu, S.; Zhan, J.; Man, B.; Jiang, S.; Yue, W.; Gao, S.; Guo, C.; Liu, H.; Li, Z.; Wang, J.; Zhou, Y. Real-time reliable determination of binding kinetics of DNA hybridization using a multi-channel graphene biosensor. *Nat. Commun.* **2017**, *8*, 14902.
(37) Ping, J.; Vishnubhotla, R.; Vrudhula, A.; Johnson, A. T. Scalable production of high-sensitivity, label-free DNA biosensors based on back-gated graphene field effect transistors. *ACS Nano* **2016**, *10* (9), 8700−8704.
(38) Hwang, M. T.; Heiranian, M.; Kim, Y.; You, S.; Leem, J.; Taqieddin, A.; Faramarzi, V.; Jing, Y.; Park, I.; van der Zande, A. M.; Nam, S.; Aluru, N. R.; Bashir, R. Ultrasensitive detection of nucleic acids using deformed graphene channel field effect biosensors. *Nat. Commun.* **2020**, *11* (1), 1543.
(39) Kwon, J.; Lee, Y.; Lee, T.; Ahn, J. H. Aptamer-based field-effect transistor for detection of avian influenza virus in chicken serum. *Anal. Chem.* **2020**, *92* (7), 5524−5531.
(40) Tian, M.; Qiao, M.; Shen, C.; Meng, F.; Wang, J. Highly-sensitive graphene field effect transistor biosensor using PNA and DNA probes for RNA detection. *Appl. Surf. Sci.* **2020**, *527*, 146839.
(41) Chen, X.; Hao, S.; Zong, B.; Liu, C.; Mao, S. Ultraselective antibiotic sensing with complementary strand DNA assisted aptamer/MoS2 field-effect transistors. *Biosens. Bioelectron.* **2019**, *145*, 111711.
(42) Dontschuk, N.; Stacey, A.; Tadich, A.; Rietwyk, K. J.; Schenk, A.; Edmonds, M. T.; Shimoni, O.; Pakes, C. I.; Prawer, S.; Cervenka, J. A graphene field-effect transistor as a molecule-specific probe of DNA nucleobases. *Nat. Commun.* **2015**, *6*, 6563.
(43) Gao, Z.; Xia, H.; Zauberman, J.; Tomaiuolo, M.; Ping, J.; Zhang, Q.; Ducos, P.; Ye, H.; Wang, S.; Yang, X.; Lubna, F.; Luo, Z.; Ren, L.; Johnson, A. T. C. Detection of sub-fM DNA with target recycling and self-assembly amplification on graphene field-effect biosensors. *Nano Lett.* **2018**, *18* (6), 3509−3515.
(44) Cheung, K. M.; Abendroth, J. M.; Nakatsuka, N.; Zhu, B.; Yang, Y.; Andrews, A. M.; Weiss, P. S. Detecting DNA and RNA and differentiating single-nucleotide variations via field-effect transistors. *Nano Lett.* **2020**, *20* (8), 5982−5990.
(45) Hwang, M. T.; Landon, P. B.; Lee, J.; Choi, D.; Mo, A. H.; Glinsky, G.; Lal, R. Highly specific SNP detection using 2D graphene electronics and DNA strand displacement. *Proc. Natl. Acad. Sci. U. S. A.* **2016**, *113* (26), 7088−7093.
(46) Nakatsuka, N.; Yang, K. A.; Abendroth, J. M.; Cheung, K. M.; Xu, X.; Yang, H.; Zhao, C.; Zhu, B.; Rim, Y. S.; Yang, Y.; Weiss, P. S.; Stojanović, M. N.; Andrews, A. M. Aptamer-field-effect transistors overcome Debye length limitations for small-molecule sensing. *Science* **2018**, *362* (6412), 319−324.
(47) Campos, R.; Borme, J.; Guerreiro, J. R.; Machado, G J. R.; Cerqueira, M. F.; Petrovykh, D. Y.; Alpuim, P. Attomolar label-free detection of DNA hybridization with electrolyte-gated graphene field-effect transistors. *ACS Sens.* **2019**, *4* (2), 286−293.
(48) Wang, S.; Zhang, L.; Wan, S.; Cansiz, S.; Cui, C.; Liu, Y.; Cai, R.; Hong, C.; Teng, I. T.; Shi, M.; Wu, Y.; Dong, Y.; Tan, W. Aptasensor with expanded nucleotide using DNA nanotetrahedra for electrochemical detection of cancerous exosomes. *ACS Nano* **2017**, *11* (4), 3943−3949.
(49) Lin, M.; Song, P.; Zhou, G.; Zuo, X.; Aldalbahi, A.; Lou, X.; Shi, J.; Fan, C. Electrochemical detection of nucleic acids, proteins, small molecules and cells using a DNA-nanostructure-based universal biosensing platform. *Nat. Protoc.* **2016**, *11* (7), 1244−1263.
(50) Falasca, F.; Sciandra, I.; Di Carlo, D.; Gentile, M.; Deales, A.; Antonelli, G.; Turriziani, O. Detection of SARS-COV N2 gene: very low amounts of viral RNA or false positive? *J. Clin. Virol.* **2020**, *133*, 104660.
(51) Duan, X.; Li, Y.; Rajan, N. K.; Routenberg, D. A.; Modis, Y.; Reed, M. A. Quantification of the affinities and kinetics of protein interactions using silicon nanowire biosensors. *Nat. Nanotechnol.* **2012**, *7* (6), 401−407.
(52) Wang, Z.; Yi, K.; Lin, Q.; Yang, L.; Chen, X.; Chen, H.; Liu, Y.; Wei, D. Free radical sensors based on inner-cutting graphene field-effect transistors. *Nat. Commun.* **2019**, *10* (1), 1544.
(53) Seo, G.; Lee, G.; Kim, M. J.; Baek, S. H.; Choi, M.; Ku, K. B.; Lee, C. S.; Jun, S.; Park, D.; Kim, H. G.; Kim, S. J.; Lee, J. O.; Kim, B. T.; Park, E. C.; Kim, S. I. Rapid detection of COVID-19 causative virus (SARS-CoV-2) in human nasopharyngeal swab specimens using field-effect transistor-based biosensor. *ACS Nano* **2020**, *14* (4), 5135−5142.
(54) Kwong Hong Tsang, D.; Lieberthal, T. J.; Watts, C.; Dunlop, I. E.; Ramadan, S.; Del Rio Hernandez, A. E.; Klein, N. Chemically functionalised graphene FET biosensor for the label-free sensing of exosomes. *Sci. Rep.* **2019**, *9* (1), 13946.
(55) Liu, Y.; Yuan, L.; Yang, M.; Zheng, Y.; Li, L.; Gao, L.; Nerngchamnong, N.; Nai, C. T.; Sangeeth, C. S.; Feng, Y. P.; Nijhuis, C. A.; Loh, K. P. Giant enhancement in vertical conductivity of stacked CVD graphene sheets by self-assembled molecular layers. *Nat. Commun.* **2014**, *5*, 5461.
(56) Huang, P. J.; Liu, J. DNA-length-dependent fluorescence signaling on graphene oxide surface. *Small* **2012**, *8* (7), 977−983.
(57) Gaudreau, L.; Tielrooij, K. J.; Prawiroatmodjo, G. E. D. K.; Osmond, J.; García de Abajo, F. J.; Koppens, F. H. L. Universal distance-scaling of nonradiative energy transfer to graphene. *Nano Lett.* **2013**, *13* (5), 2030−2035.
(58) Hwang, M. T.; Wang, Z.; Ping, J.; Ban, D. K.; Shiah, Z. C.; Antonschmidt, L.; Lee, J.; Liu, Y.; Karkisaval, A. G.; Johnson, A. T. C.; Fan, C.; Glinsky, G.; Lal, R. DNA nanotweezers and graphene transistor enable label-free genotyping. *Adv. Mater.* **2018**, *30*, e1802440.
(59) Anichini, C.; Czepa, W.; Pakulski, D.; Aliprandi, A.; Ciesielski, A.; Samorì, P. Chemical sensing with 2D materials. *Chem. Soc. Rev.* **2018**, *47* (13), 4860−4908.
(60) Kaisti, M. Detection principles of biological and chemical FET sensors. *Biosens. Bioelectron.* **2017**, *98*, 437−448.
(61) Chen, T. Y.; Loan, P. T.; Hsu, C. L.; Lee, Y. H.; Tse-Wei Wang, J.; Wei, K. H.; Lin, C. T.; Li, L. J. Label-free detection of DNA hybridization using transistors based on CVD grown graphene. *Biosens. Bioelectron.* **2013**, *15* (41), 103−109.
(62) Dong, X.; Shi, Y.; Huang, W.; Chen, P.; Li, L. J. Electrical detection of DNA hybridization with single-base specificity using transistors based on CVD-grown graphene sheets. *Adv. Mater.* **2010**, *22* (14), 1649−1653.
(63) Sips, R. On the structure of a catalyst surface. *J. Chem. Phys.* **1948**, *16* (5), 490−495.
(64) Yu, F.; Yao, D.; Knoll, W. Oligonucleotide hybridization studied by a surface plasmon diffraction sensor (SPDS). *Nucleic Acids Res.* **2004**, *32* (9), e75.
(65) Halperin, A.; Buhot, A.; Zhulina, E. B. Sensitivity, specificity, and the hybridization isotherms of DNA chips. *Biophys. J.* **2004**, *86* (2), 718−730.
(66) Barak, N.; Ben-Ami, R.; Sido, T.; Perri, A.; Shtoyer, A.; Rivkin, M.; Licht, T.; Peretz, A.; Magenheim, J.; Fogel, I.; Livneh, A.; Daitch, Y.; Oiknine-Djian, E.; Benedek, G.; Dor, Y.; Wolf, D. G.; Yassour, M. Hebrew university-hadassah COVID-19 diagnosis team. Lessons from applied large-scale pooling of 133,816 SARS-CoV-2 RT-PCR tests. *Sci. Transl. Med.* **2021**, *13* (589), eabf2823.
(67) Zhao, H.; Liu, F.; Xie, W.; Zhou, T. C.; OuYang, J.; Jin, L.; Li, H.; Zhao, C. Y.; Zhang, L.; Wei, J.; Zhang, Y. P.; Li, C. P. Ultrasensitive supersandwich-type electrochemical sensor for SARS-

CoV-2 from the infected COVID-19 patients using a smartphone. *Sens. Actuators, B* **2021**, *327*, 128899.
(68) Chaibun, T.; Puenpa, J.; Ngamdee, T.; Boonapatcharoen, N.; Lertanantawong, B. Rapid electrochemical detection of coronavirus SARS-CoV-2. *Nat. Commun.* **2021**, *12*, 802.
(69) WHO. Transmission of SARS-CoV-2: implications for infection prevention precautions. https://www.who.int/news-room/commentaries/detail/transmission-of-sars-cov-2-implications-for-infection-prevention-precautions (accessed June 18, 2021).
(70) Wang, W.; Xu, Y.; Gao, R.; Lu, R.; Han, K.; Wu, G.; Tan, W. Detection of SARS-CoV-2 in different types of clinical specimens. *JAMA* **2020**, *323* (18), 1843−1844.
(71) Jiao, C.; Sharma, S.; Dugar, G.; Peeck, N. L.; Bischler, T.; Wimmer, F.; Yu, Y.; Barquist, L.; Schoen, C.; Kurzai, O.; Sharma, C. M.; Beisel, C. L. Noncanonical crRNAs derived from host transcripts enable multiplexable RNA detection by Cas9. *Science* **2021**, *372* (6545), 941−948.
(72) Smyrlaki, I.; Ekman, M.; Lentini, A.; Rufino de Sousa, N.; Papanicolaou, N.; Vondracek, M.; Aarum, J.; Safari, H.; Muradrasoli, S.; Rothfuchs, A. G.; Albert, J.; Högberg, B.; Reinius, B. Massive and rapid COVID-19 testing is feasible by extraction-free SARS-CoV-2 RT-PCR. *Nat. Commun.* **2020**, *11* (1), 4812.
(73) Li, Y.; Tseng, Y. D.; Kwon, S. Y.; D'Espaux, L.; Bunch, J. S.; McEuen, P. L.; Luo, D. Controlled assembly of dendrimer-like DNA. *Nat. Mater.* **2004**, *3* (1), 38−42.
(74) Li, Y.; Cu, Y. T.; Luo, D. Multiplexed detection of pathogen DNA with DNA-based fluorescence nanobarcodes. *Nat. Biotechnol.* **2005**, *23* (7), 885−889.

https://doi.org/10.1021/jacs.1c06325
J. Am. Chem. Soc. 2021, 143, 17004−17014